Bollettino di Geofisica Teorica ed Applicata Vol. 61, n. 4, pp. 451-468; December 2020
DOI 10.4430/bgta0322

Regional seismicity in Adıyaman - Samsat (SE Turkey)

T.S. Irmak[1], İ. Bulut[1] and B. Doğan[2]

[1] *Dept. of Geophysics, Seismology Section, University of Kocaeli, Turkey*
[2] *Dept. of Geology, University of Kocaeli, Turkey*

(Received: 4 November 2019; accepted: 9 February 2020)

ABSTRACT Earthquake locations in Turkey are reported by two different agencies: Disaster and Emergency Management Presidency (DEMP) and Kandilli Observatory and Earthquake Research Institute (KOERI). Both organisations use their own networks. Thus, different parameters are usually given for the same earthquake due to the differences in the number of stations and network designs. This makes it difficult to obtain a reliable regional earthquake source parameters' database catalogue. This study aims to relocate the earthquakes that occurred in Adıyaman-Samsat by using DEMP and KOERI stations records, determine the fault mechanisms and define the fault mechanism in relation to the regional tectonics, as well as provide a stable regional source parameters' database. For this purpose, 434 earthquakes ($M \geq 1.3$) were relocated by combining DEMP and KOERI data, and the focal mechanisms of 32 earthquakes ($M \geq 3.5$) from P-wave first motion polarities and of 25 earthquakes ($M \geq 3.6$) from regional moment tensor analysis have been determined. All these events occurred in the study area during 2009-2018. The new locations of the earthquakes indicated that the earthquakes are clustered in the Samsat peninsula, at the SW part of the Bozova Fault. Additionally, some scattering epicentres were observed in the southern part of the study area. It was determined that earthquakes mainly occurred in the land areas rather than at the Atatürk Dam and at Samsat peninsula, at very shallow depths (mostly within the first 10 km of the crust). The depth distribution of the analysed earthquakes indicated that both the maximum seismicity and depth of the seismicity increased from south to north and this behaviour indicates crustal thickening due to continental-continental collision in the study area. Focal mechanisms of the analysed earthquakes showed that the dominant mechanism in the study area was NW-SE trending right lateral strike-slip faulting with both normal and reverse component. All the focal mechanisms had a NW-SE or NE-SW nodal plane compatible with the regional geological trend at the NE edge of the Samsat Peninsula, where the left lateral strike slip Lice Fault and Samsat Fault intersect. However, the identification of Samsat Fault as the main seismic source is strongly supported by the 2017 and 2018 seismic sequences in the study area.

Key words: Arabian plate, SE Turkey, Samsat Fault, Lice Fault, relocation, moment tensor.

1. Introduction

The plate movements in Anatolia during Plio-Quaternary began to take place following the continental-continental collision with the northward movement (~20 mm/year) of the Arabian plate (Reilinger *et al.*, 2006). This collision allowed the development of the Bitlis-Zagros Suture Zone (BZSZ) in the eastern and south-eastern Anatolia regions (Fig. 1). As a result of the continental-continent collision, the BZSZ was identified as the primary structural element causing the thickening of the continental crust in the region due to the shortening of the eastern Anatolian region in the N-S direction. The tectonic structure of the study area is shaped as a result of the movement of the Arabian plate and the Eurasian plate as in the entire SE Anatolia region (Fig. 1). The most prominent tectonic structures in the region are the Adıyaman Fault, Bozova Fault, Lice Fault, and Kalecik Fault (Perinçek and Çemen, 1990; Taymaz *et al.*, 1991; Ertunç, 1999). However, there is a dearth of literature and reports with regards to the subject matter in the study area and its environs (Şahbaz and Seyitoğlu, 2018; Kartal and Kadirioğlu, 2019; Tatar *et al.*, 2019).

Analysis of seismicity is useful to constrain dominant seismic activity in a fault system. The accurate estimation of hypocentral parameters, seismic moments, fault plane systems, and the orientation of the P and T axes derived from focal mechanism are very useful in understanding the regional seismicity, tectonics, and kinematics in a region. In addition, the presence of monumental engineering structures such as the Atatürk Dam makes it imperative to obtain a more reliable earthquake source parameters database in the region. The Atatürk Dam is the 4th largest dam in

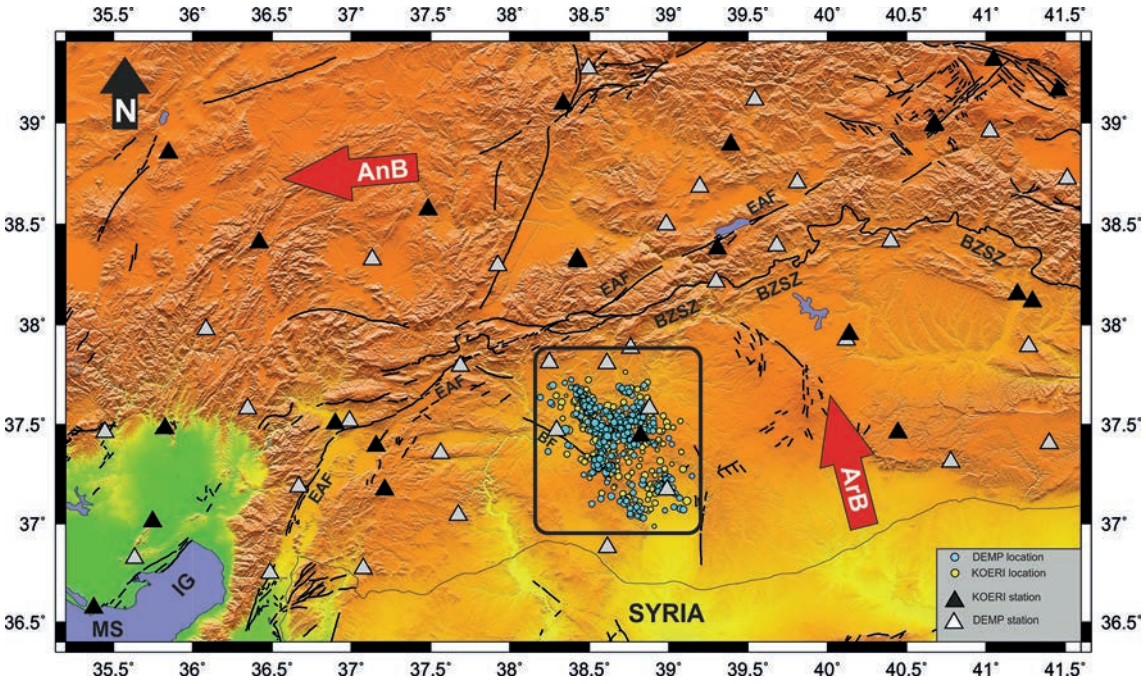

Fig. 1 - Tectonic settings of the study area. EAF: East Anatolian Fault, BZSZ: Bitlis-Zagros Suture Zone, BF: Bozova Fault, MS: Mediterranean Sea, IG: Iskenderun Gulf. Red arrows show plate movement direction with respect to the Eurasian plate (ArB: Arabian Block, AnB: Anatolian Block). The study area is shown by a black rectangle.

the world in terms of structure volume. The hydroelectric power plant is the 5th largest power plant in the world in terms of installed capacity (MW). The dam is also noted as the largest dam in Turkey as well as in Europe.

In general, Turkey and its surroundings are characterised by high seismic activity. However, it has been established that some areas have lower seismic activity than its surrounding areas. In fact, one of the main reasons for a region to appear to have a low seismic activity has been attributed to the small number of earthquake recording stations in the region. Following the earthquakes in 1999 [17 August 1999 Kocaeli (M_W = 7.4) and 12 November 1999 Düzce (M_W = 7.2)] along with the increasing number of seismograph stations installed in Turkey, different seismic behaviours in many parts of the country began to be evident. Thus, it has become important to conduct studies on the seismic activities of the areas, which were not studied previously. The study area, Adıyaman-Samsat, is considered to be one of those areas.

Earthquake locations in Turkey are usually reported by two different agencies, the Disaster and Emergency Management Presidency (DEMP) and Kandilli Observatory and Earthquake Research Institute (KOERI). Both organisations use their own networks. As a result, different parameters are given for the same earthquake due to the differences in the number of stations and network designs. It is therefore difficult to obtain a reliable regional earthquake source parameters' database. In 2006, there were only 11 seismograph stations operated by KOERI and DEMP within the 200 km radius of Samsat, which increased to 40 in 2018 (Fig. 2). Considering the seismic activity of the study area and its surroundings, there have been 23 reported earthquakes larger than 5 ($M \geq 5.0$) from the 1900s to date (Table 1).

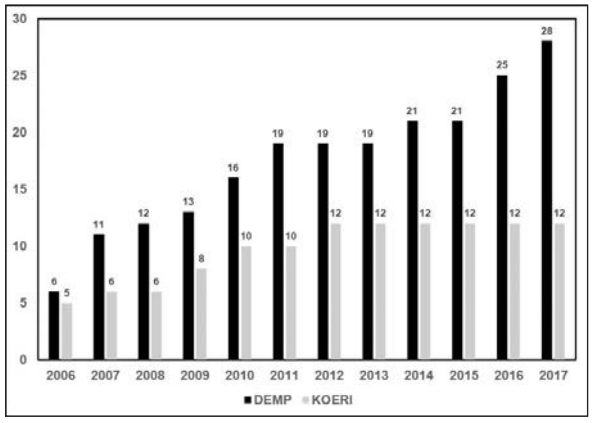

Fig. 2 - Changes in the number of stations operated by DEMP and KOERI within the 200 km radius of the Samsat town by years.

This study aims to relocate the earthquakes that occurred in the study area by using DEMP and KOERI station records, determine the fault mechanisms and define the fault mechanism in relation to the regional tectonics, as well as provide a stable regional source parameters' database. To this end, 434 earthquakes ($M \geq 1.3$) were relocated by combining DEMP and KOERI data and the focal mechanisms of 32 earthquakes ($M \geq 3.5$) from P-wave first motion polarities were computed. The focal mechanism of the 32 earthquakes ($M \geq 3.5$) were determined from P-wave first motion polarities, out of which 25 earthquakes ($M \geq 3.6$) were determined from regional moment tensor analysis. It should be noted that these events occurred in the study area over

Table 1 - Seismic activity of the study area and vicinity from the 1900s until today.

Date	Time	Lat (°)	Lon (°)	Depth (km)	Magnitude (*xM*)	Location
1914.10.04	18:48:57.70	38.0100	38.2400	15.0	5.3	Çelikhan-Adıyaman
1915.05.19	04:48:02.40	37.6200	39.4700	10.0	5.5	Siverek-Şanlıurfa
1931.01.09	07:01:35.00	38.0000	38.5000	30.0	5.2	Sincik-Adıyaman
1931.05.06	20:22:25.00	37.5000	39.5000	30.0	5.3	Siverek-Şanlıurfa
1936.02.02	17:08:26.10	37.6900	38.8200	16.0	5.3	Hilvan-Şanlıurfa
1940.12.20	05:18:00.00	38.3000	38.3000	10.0	5.8	Yeşilyurt-Malatya
1949.04.25	23:09:21.00	38.2700	38.9900	80.0	5.5	Doğanyol-Malatya
1950.05.09	09:20:10.60	38.2400	38.3200	70.0	5.3	Yeşilyurt-Malatya
1950.11.08	10:08:01.50	38.2700	39.1600	50.0	5.4	Güngüş-Diyarbakır
1964.04.23	14:23:47.60	38.0900	38.7500	57.0	5.3	Pütürge-Malatya
1964.06.14	12:15:31.40	38.1300	38.5100	3.0	6.0	Sincik-Adıyaman
1964.06.14	12:38:03.00	37.9800	38.5100	30.0	5.0	Sincik-Adıyaman
1965.05.16	11:29:04.10	38.1600	38.9800	26.0	5.2	Pütürge-Malatya
1968.10.30	16:51:35.20	37.9900	38.5600	3.0	5.3	Sincik-Adıyaman
1981.01.20	08:27:49.00	38.0500	38.5900	24.0	5.0	Sincik-Adıyaman
1986.05.05	03:35:38.00	38.0200	37.7900	4.0	5.8	Doğanşehir-Malatya
1986.06.06	10:39:47.00	38.0100	37.9100	11.0	5.6	Doğanşehir-Malatya
2003.07.13	01:48:21.60	38.3300	38.9800	6.0	5.6	Sivrice-Elazığ
2004.02.26	04:13:57.70	38.0100	38.2400	6.0	5.0	Çelikhan-Adıyaman
2005.11.26	15:56:55.78	38.2897	38.8255	9.4	5.3	Pütürge-Malatya
2008.09.03	02:22:47.83	37.5092	38.4985	5.7	5.1	Samsat-Adıyaman
2017.03.02	11:07:24.37	37.4860	38.5010	14.6	5.7	Kasımkuyu-Şanlıurfa
2018.04.24	00:34:29.15	37.5217	38.5032	13.2	5.4	Samsat-Adıyaman

* *xM* = maximum magnitude values reported by KOERI among others, m_b, M_s, M_w, M_L

the last decade (from 2009 to 2018) and have been presented in this study. Within this scope, phase readings were conducted again, employing both regionally recorded seismic waves and first motion polarities, and regional moment tensor analysis to extract information about the earthquake sources, in particular, depth, seismic moment, and focal mechanism. HYPO71 (Lee and Lahr, 1975) was used for the relocation process, while different methodologies for the determination of fault plane mechanisms were applied. First, the well-known search method employed by Snoke *et al*. (1984) was applied on the P-wave first motion data of 32 earthquakes. Then, the waveform matching method of Pasyanos *et al*. (1996) and Dreger (2003) was used for 25 ($M \geq 3.6$) suitable earthquakes.

2. Tectonic setting

The south-eastern Anatolia region is a fore-arc basin where the Neotethys oceanic lithosphere was depleted by subduction until the beginning of the Late Cretaceous and Miocene. The study

area mainly consists of sedimentary rocks (Yılmaz *et al*., 1993). The continental crust of the study area was affected by the movement of the Arabian plate from the Miocene (20 Myr) and the primary deformation of the Arabian-Anatolian plates with the continental-continental collision (Okay *et al*., 2010). These tectonic domains have been subjected to both compression and deformation with strike slip faulting. The tectonic mechanism responsible for earthquake occurence in the study area is due to two transcurrent faults: the right lateral strike slip Samsat Fault and the left lateral strike slip Lice Fault. The Samsat Fault has a length of 12 km with a NW-SE direction, which varies between N20° and 55°E in the region, dipping to both north and south. The other oblique normal faults observed in the zones formed along with this fault are dipping in two directions. On the other hand, the Lice Fault is oriented generally in a NE-SW direction in areas close to the coast of Atatürk Dam and is prominent within Germav and Gercüş formations (Fig. 3). The Samsat Fault is towards the south of the Atatürk Dam, and the continuation of the north of Urfa is the Kalecik Fault (Perinçek *et al*., 1987; İmamoğlu *et al*., 2017; Özcan *et al*., 2017). The Bozova Fault is one of the youngest faults found in the SE of the Samsat district. The Bozova Fault is another right lateral strike-slip, which is associated with the deformation of the crust in the region. The main tectonic features in the study area include the Samsat, Lice, Bozova, and Kalecik faults and these provide important information about the deformation of the continental crust.

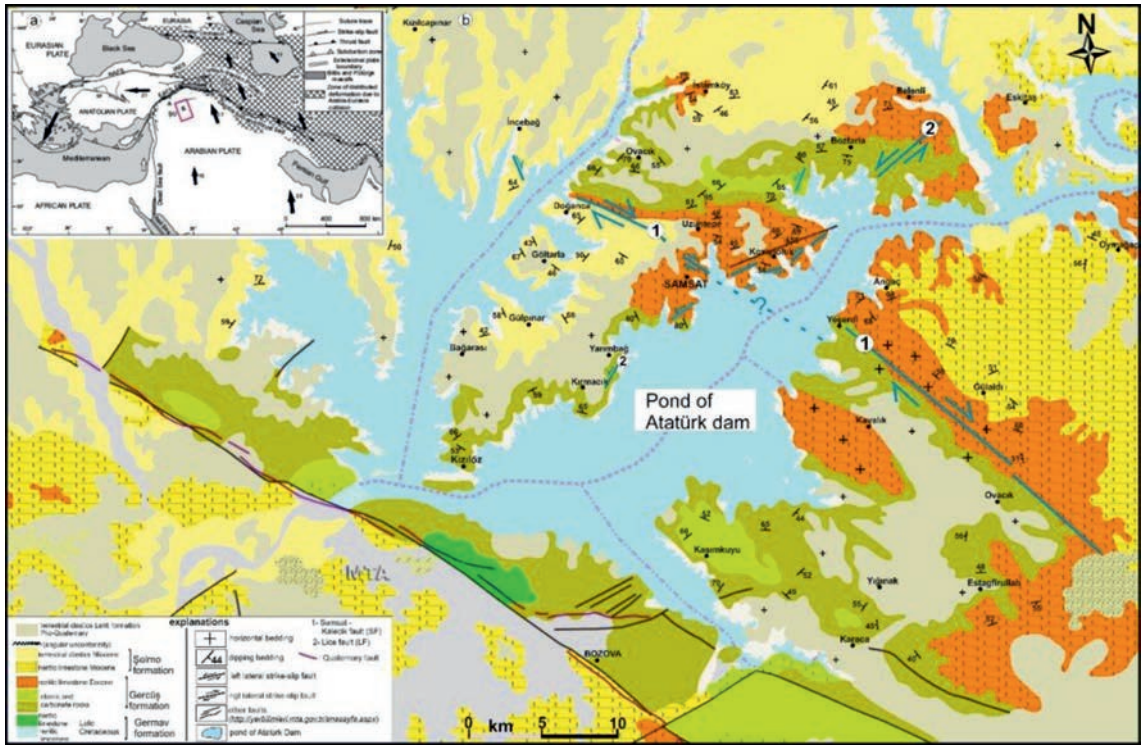

Fig. 3 - Detailed geological map of the study area and its surroundings. The study area is shown by the red square in the large scale map in the left corner.

3. Seismological studies

3.1. Relocation of the earthquakes

The number of seismograph stations installed and operated by DEMP and KOERI in the eastern and western part of Turkey differs significantly. Although there has been an increase in the number of stations installed by DEMP in the eastern part of Turkey in recent years, there are still differences between the two organisation networks in terms of design and number of stations. These differences have significant effects on the locations of the earthquakes. Fig. 4 shows the locations given by KOERI and DEMP for the same earthquakes that occurred between 2009 and 2018. Additionally, the location algorithm used by the organisations could be another reason for

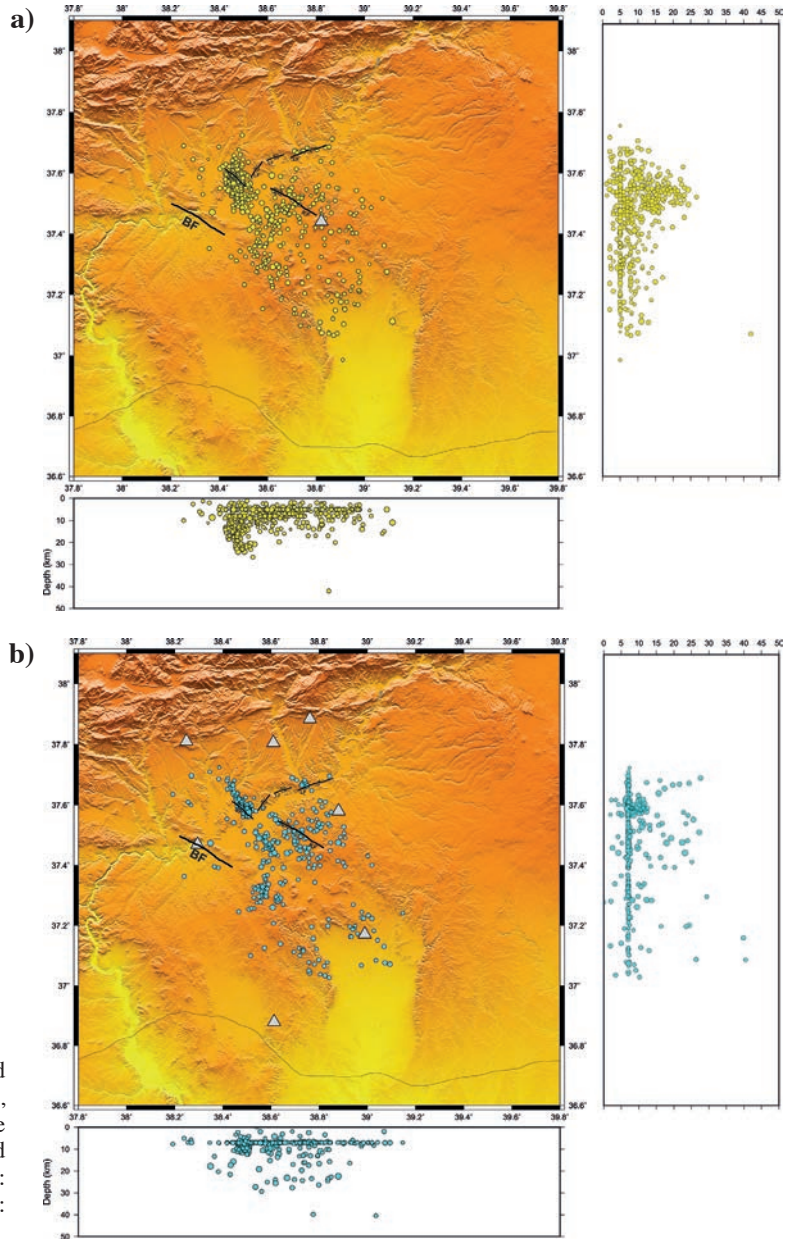

Fig. 4 - Location of the analysed earthquakes reported by KOERI (a), and DEMP (b). Triangles indicate stations belonging to KOERI and DEMP, BF: Bozova Fault, SF: Samsat Fault, LF: Lice Fault, KF: Kalecik Fault.

the differences. KOERI has been adopting HYPO71 (Lee and Lahr, 1975) which uses the least squares method to locate earthquakes, while DEMP uses HYPOCENTER which employs the damped least squares method (Lienert *et al*, 1986). Therefore, more scattered earthquakes in the KOERI catalogue seem to be compatible with active faults in the DEMP catalogue. Even though the DEMP catalogue seems compatible with active tectonics, the depth distribution of the DEMP catalogue indicated that most of earthquake depths are fixed to 5-7 km. This is probably due to insufficient or inaccurate S-phase reading.

In this study, data from KOERI and DEMP stations of the same earthquake were combined for the 434 earthquakes ($M > 1.3$) occurring after 2009. HYPO71 algorithm, which uses P- and S-wave travel times, was used in the analysis and all phase picking was done manually. A layered P-velocity model was used and the V_P/V_S ratio taken as 1.73 (Kalafat *et al*., 1987). Four hundred thirty-four well-located events were obtained with local magnitudes ranging from 1.3 to 5.4.

3.2. Fault plane solution (P-wave first motion)

The Focmec program, which uses P-wave polarities on vertical component seismograms, was used to calculate the fault plane solutions (Snoke *et al*., 1984). All available P-wave polarities on vertical seismograms obtained from KOERI and DEMP were recorded. The number of stations with unambiguous first arrival polarities varied from earthquake to earthquake; however, events with fewer than 10 clear polarity readings as well as those with ambiguous polarities were discarded. Additionally, solutions with stations only in 3 quadrants of the focal mechanism were not included in the final result. In the case of low S/N ratio, the P waves were converted to displacement in order to better observe the P-wave onsets. Biasing calculation of azimuth and take off angle, and aliasing effects as well as polarity errors can occur on the seismograms due to structural heterogeneity (Scherbaum, 1994). However, no polarity error was allowed in the solutions. Therefore, the results obtained were only for relatively large earthquakes ($M > 3.5$). Events with multiple acceptable solutions indicating different mechanisms or with faulting parameter uncertainties exceeding 20° were also not reported in this study. Fig. 5 gives an example of the first motion focal mechanism solution for the 24 March 2018, 00:34:27 ($M_W = 5.4$) event. The source parameters obtained are given in Table 2.

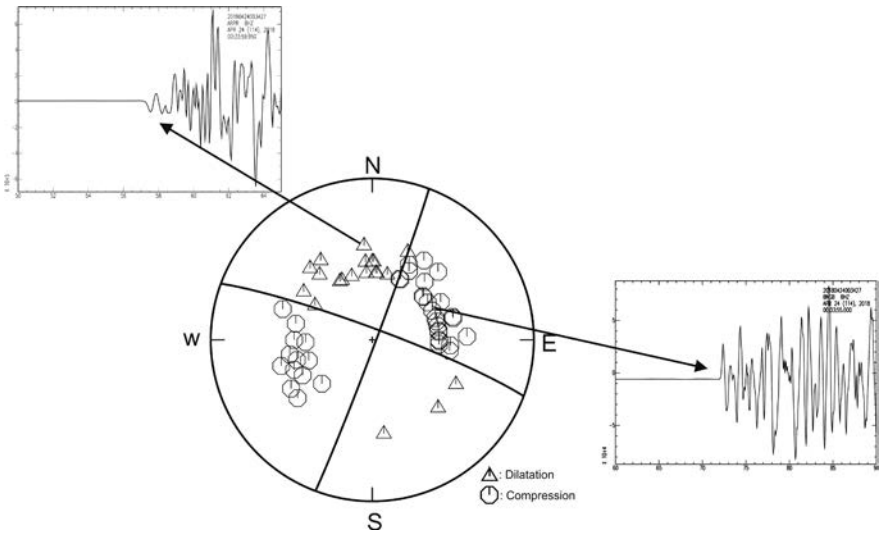

Fig. 5 - Focal mechanism solution for the 24 April 2018 00:34:27 ($M_W = 5.4$) event.

Table 2 - Source parameters of analysed earthquakes obtained from P-wave first motion analysis.

	Date-Time	Lat (°)	Lon (°)	Depth (km)	Magnitude (M_L*)	Strike (°)	Dip (°)	Slip/rake (°)
1	19.05.2009-06:53:40	37.6777	38.7100	7.1	3.5	20	34	-47
2	09.12.2009-15:54:42	37.6547	38.4228	5.7	3.5	343	29	-22
3	30.04.2010-17:03:00	37.5410	38.8627	5.2	3.5	245	52	68
4	01.12.2012-03:51:42	37.4843	38.3482	7.9	4.0	342	47	-88
5	13.08.2015- 04:14:24	37.2933	38.6300	3.8	3.7	35	67	30
6	10.11.2015- 07:59:40	37.2755	38.6383	5.0	3.8	72	39	88
7	13.12.2016-21:01:08	37.5965	38.5038	7.6	3.7	237	71	54
8	02.03.2017-11:07:24	37.5947	38.4612	5.0	5.7	39	79	7
9	02.03.2017-11:16:54	37.601	38.4465	1.8	3.8	25	68	-12
10	02.03.2017-11:18:16	37.5882	38.4672	1.9	4.3	5	43	-81
11	02.03.2017-11:24:15	37.6187	38.4995	5.0	4.2	6	44	-69
12	02.03.2017-13:44:11	37.6013	38.4667	6.3	4.0	210	82	-36
13	02.03.2017-13:47:13	37.6395	38.4648	5.4	3.7	16	41	-54
14	02.03.2017-14:55:19	37.6175	38.5025	5.0	3.6	55	44	65
15	02.03.2017-16:44:10	37.5902	38.4807	6.0	3.5	16	21	-12
16	02.03.2017-16:45:15	37.588	38.4895	1.8	3.9	14	41	-68
17	02.03.2017-23:10:53	37.622	38.4715	8.8	3.8	226	56	-10
18	03.03.2017-20:51:53	37.6217	38.4702	6.5	3.9	36	62	-48
19	04.03.2017-04:00:41	37.6165	38.4677	3.0	3.7	33	83	1
20	05.03.2017-06:26:20	37.5867	38.5022	3.6	3.5	32	70	-26
21	08.03.2017-11:26:48	37.6127	38.4787	2.2	3.5	46	86	-31
22	08.03.2017-22:31:24	37.6257	38.4610	3.8	3.6	49	80	-13
23	10.03.2017-22:23:42	37.5818	38.5110	5.7	4.2	31	76	-35
24	14.03.2017-10:30:06	37.5947	38.4962	3.2	3.7	216	75	-8
25	19.03.2017-07:01:52	37.6172	38.4657	3.4	3.7	44	86	-29
26	26.04.2017-08:26:40	37.5945	38.4873	2.4	3.6	31	67	-30
27	27.04.2017-09:50:59	37.5990	38.4990	5.0	3.7	47	88	-29
28	02.05.2017-20:38:04	37.5883	38.5223	1.5	3.7	213	71	-2
29	25.12.2017-17:40:41	37.2903	38.6377	5.9	3.8	64	89	30
30	24.04.2018-00:34:27	37.5718	38.5083	1.0	5.5	20	88	5
31	24.04.2018-04:50:48	37.6185	38.4768	9.6	3.7	252	83	-90
32	21.05.2018-01:09:23	37.4558	38.6137	1.7	4.2	214	63	16

* M_L reported by KOERI

3.3. Time domain moment tensor analysis

An inversion scheme was performed following the least squares approach by Dreger and Helmberger (1993) and Dreger (2003), who demonstrated that the method is reliable for events with local magnitudes as low as 3.5 and this was used to obtain focal mechanism solutions for the analysed earthquakes in the study area. Three-component body waveforms recorded at local

and regional distances were used to determine the seismic moment tensor with this technique. The essence of this procedure design was to obtain reliable solutions using a minimal number of stations and data from a single three-component station. In most cases, a few stations with some azimuthal coverage may generally give more reliable results (Dreger and Helmberger, 1991, 1993; Romanowicz *et al*., 1993; Gee *et al*., 1996; Shomali and Slunga, 2000; Irmak, 2013, 2016).

The source time function applied in this study was assumed to be a Dirac delta function since the events generally have source durations of 2–3 s (M_L < 5) and seismograms in the passband of 20-50 s (Dreger, 2003). The results of the moment tensor inversion are generally not very sensitive to location errors. Errors of up to 15 km in epicentre locations are less important at a distance range of 50-400 km (Dreger and Helmberger, 1993; Pasyanos *et al*., 1996). The depth of the source was found iteratively by finding the solution that yields the largest variance reduction.

Green's functions were calculated following a modified Haskell algorithm in the frequency-wavenumber domain (Saikia, 1994). The formulation uses the three basic focal mechanisms: normal, reverse, and pure strike-slip (Langston, 1981; Herrmann and Wang, 1985). Far-field and near-field terms were both considered in this algorithm. The sampling rate was fixed at 2 Hz. The velocity model employed by Kalafat *et al*. (1987) was used.

The quality of the inversion can be controlled by different functions. Dreger *et al*. (1995) and Dreger and Kaverina (2000) indicated that output data variance and variance reduction assumes a value of 100 when observed and calculated seismograms are identical. Furthermore, the resulting tensor can be decomposed into a double-couple (DC) and a Compensated Linear Vector Dipole (CLVD). The percentage of DC (PDC) (Jost and Herrmann, 1989) shows how well the model complies with a double-couple source. However, CLVD contribution is assumed to be an artifact of the present inversion scheme and indicates the influences of structural complexities. The CLVD contribution was not considered in the calculation of the Green's functions, source complexities, location errors (depth), etc.

3.3.1. Data processing

Data selected at regional distance were retrieved via the Internet from the KOERI data centre in SAC format (KOERI, 2019). The three-component broadband seismograms were divided into predefined time segments and converted to ground displacement using poles and zeros. Prior to conversion of displacement using the trapezoidal rule (within SAC), the linear trend was removed with the data tapered and rotated into a ray coordinate system. Magnitude dependent frequency bands were applied to the waveforms in the order of $3.5<M_L<4.0$ corresponding to the frequency band 0.02-0.10 Hz; $4.0<M_L<5.0$ to 0.02-0.05 Hz, and $M \geq 5.0$ to 0.01-0.05 Hz, respectively (Dreger *et al*., 1995). To avoid phase shift, a second-order Butterworth bandpass filter was applied in both forward and backward direction. The data analysed were resampled to 2 Hz and the synthetic data finally had to be time corrected (zero-offset) to compensate for errors in the overall velocity model, source depth, etc. Fig. 6 shows an example of the regional moment tensor analysis solution for the 2 March 2017 11:07:24 (M_W = 5.4) event. The obtained source parameters are given in Table 3.

3.5. Stress inversion

Regional stress field and how these stresses act on existing structures in the crust is given by focal mechanism solutions of earthquakes that occur in the brittle part of the crust. The only

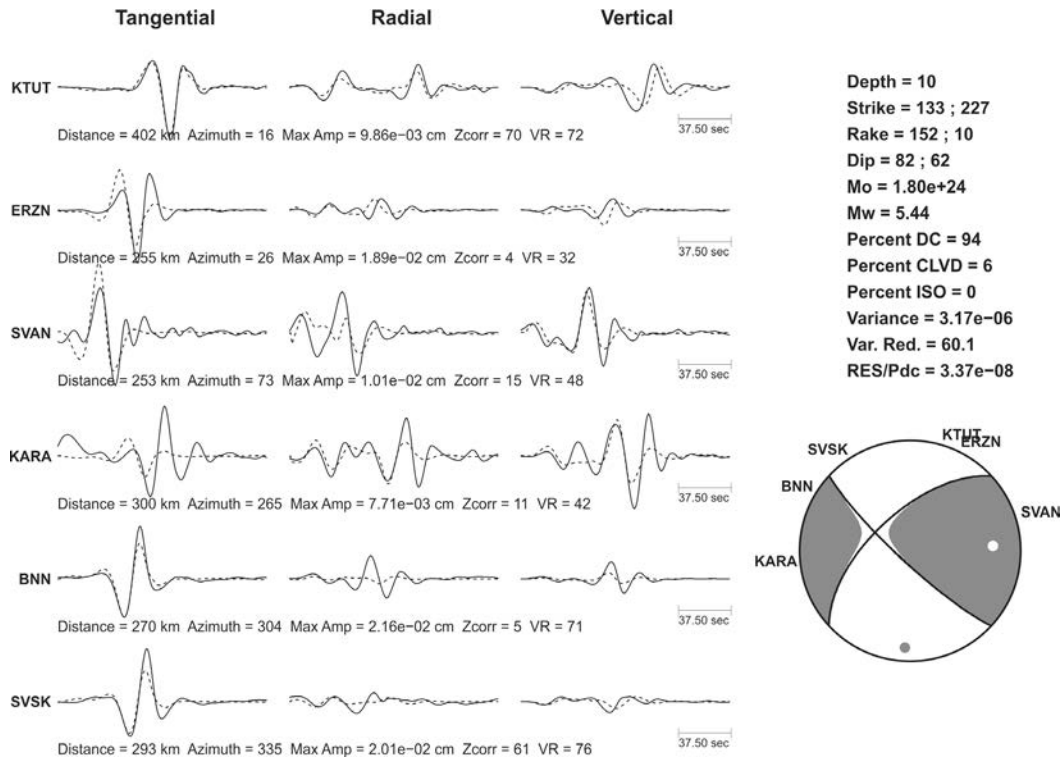

Fig. 6 - Regional moment tensor analysis of the 2 March 2017 11:07:24 (M_W = 5.4) event.

tool for *in-situ* stress measurements in the case of unavailability of borehole measurements is the analysis of the focal mechanism. In this study, the Windows version of the TENSOR program (Delvaux, 1993) developed according to the procedure described in Delvaux and Sperner (2003) with the Quality Ranking scheme as in the World Stress Map project (Sperner *et al*., 2003) was used for formal stress inversions of the given focal mechanism. These inversions are determined by first motion polarity and regional moment tensor analysis to obtain the present-day stress field for the Samsat peninsula.

The Win-Tensor program runs were based on two major assumptions for the studied region: a) the stress field is uniform and invariant in space and time; and b) earthquake slip d occurs in the direction of maximum shear stress τ (Bott, 1959). The angle between the calculated stress τ and the slip vector d is the misfit angle α. Thus, the corresponding misfit function to be minimised for each earthquake i is the misfit angle α:

$$f(i) = a(i). \tag{1}$$

The orientation of the three orthogonal principal stress axes σ_1, σ_2, and σ_3 (where $\sigma_1 \geq \sigma_2 \geq \sigma_3$) and the stress ratio R is given by:

$$R = (\sigma_2 - \sigma_3)/(\sigma_1 - \sigma_3) \tag{2}$$

which expresses the magnitude of σ_2 relative to the magnitudes of σ_1 and σ_3.

Table 3 - Source parameters of the analysed earthquakes obtained from regional moment tensor analysis.

	Date-Time	Lat (°)	Lon (°)	Magnitude (M_w)	Strike (°)	Dip (°)	Slip/ Rake (°)	Seismic Moment (dyn.cm)
1	21.02.2008-09:09:22	37.5735	38.4952	3.6	217	66	62	3.6x1021
2	03.09.2008-02:22:47	37.4677	38.5315	5.3	220	87	16	1.1x1024
3	04.09.2008-22:54.32	37.4453	38.5070	4.6	56	69	59	1.0x1023
4	29.09.2008-20:54:56	37.4768	38.5362	3.8	308	90	155	6.3x1021
5	12.02.2012-04:49:07	37.4980	38.6610	4.3	221	83	-29	3.2x1022
6	17.04.2015-11:49:57	37.4982	38.7122	3.9	138	86	169	7.5x1021
7	13.08.2015-04:14:24	37.2933	38.6300	3.7	132	82	163	4.3x1021
8	13.12.2016-23:54:15	37.6013	38.4793	3.5	306	90	-17	2.0x1021
9	02.03.2017-11:07:24	37.5947	38.4612	5.4	133	82	152	1.8x1024
10	02.03.2017-17:03:02	37.5960	38.4760	4.1	150	78	-155	2.0x1022
11	02.03.2017-23:10:53	37.6220	38.4715	3.8	134	78	-164	5.8x1021
12	03.03.2017-05:04:55	37.5795	38.5120	4.2	68	89	19	2.4x1022
13	03.03.2017-20:51:53	37.6217	38.4702	3.8	49	72	24	6.4x1021
14	03.03.2017-21:30:38	37.6217	38.4602	3.7	50	78	24	4.2x1021
15	08.03.2017-22:31:24	37.6257	38.4610	3.6	329	71	-158	3.2x1021
16	09.03.2017-17:59:23	37.5918	38.5005	3.8	306	86	-174	5.6x1021
17	10.03.2017-22:23:42	37.5818	38.5110	4.3	129	73	-134	3.6x1022
18	14.03.2017-11:41:42	37.6248	38.4652	4.0	319	77	161	1.4x1022
19	19.03.2017-07:01:52	37.6172	38.4657	3.9	304	81	-169	7.6x1021
20	02.05.2017-20:38:04	37.5883	38.5223	3.8	232	83	30	5.3x1021
21	01.07.2017-04:07:48	37.5858	38.4958	3.9	307	80	-155	7.7x1021
22	02.11.2017-07:58:32	37.5677	38.5245	3.7	136	66	-148	4.3x1021
23	25.12.2017-17:40:41	37.2903	38.6377	3.8	246	90	-27	6.6x1021
24	24.04.2018-00:34:27	37.5718	38.5083	5.4	210	78	-19	1.7x1024
25	28.07.2018-03:00:57	37.5822	38.4937	3.9	184	89	-6	8.5x1021

The main stress regime is a function of the orientation of the principal axes and the shape of the stress ellipsoid i.e. extensional when σ_1 is vertical, strike-slip when σ_2 is vertical, and compressional when σ_3 is vertical. For each of these three regimes, the value of the stress ratio R fluctuates between 0 and 1 [refer to Delvaux and Sperner (2003) for more details].

In the first step of the algorithm, both nodal planes for each earthquake were inverted to a stress tensor. In the second step, the plane best explained by the stress tensor was selected from the two nodal planes and considered as the actual focal plane. Finally, after this separation, the final inversion included only focal planes that were best fitted by a uniform stress field (Gephart and Forsyth, 1984). The graphical output of the stress tensor in an equal-area projection allowed evaluating the overall quality of the result.

4. Results and discussion

As indicated earlier, KOERI and DEMP epicentre locations of the analysed earthquakes are quite different from each other. In this study, both KOERI and DEMP stations data were combined and phase readings were reconstructed. Fig. 7 shows all 434 earthquakes relocated by using KOERI and DEMP data. Fig. 8 shows a comparison of the epicentres and hypocentres located by KOERI and DEMP obtained in this study.

The results obtained in the analysis of this study are highly reliable and compatible with the linearity and tectonics in the region, with a considerable decrease in the number of earthquakes in the Atatürk Dam. The epicentral distribution of all relocated events showed that most of the

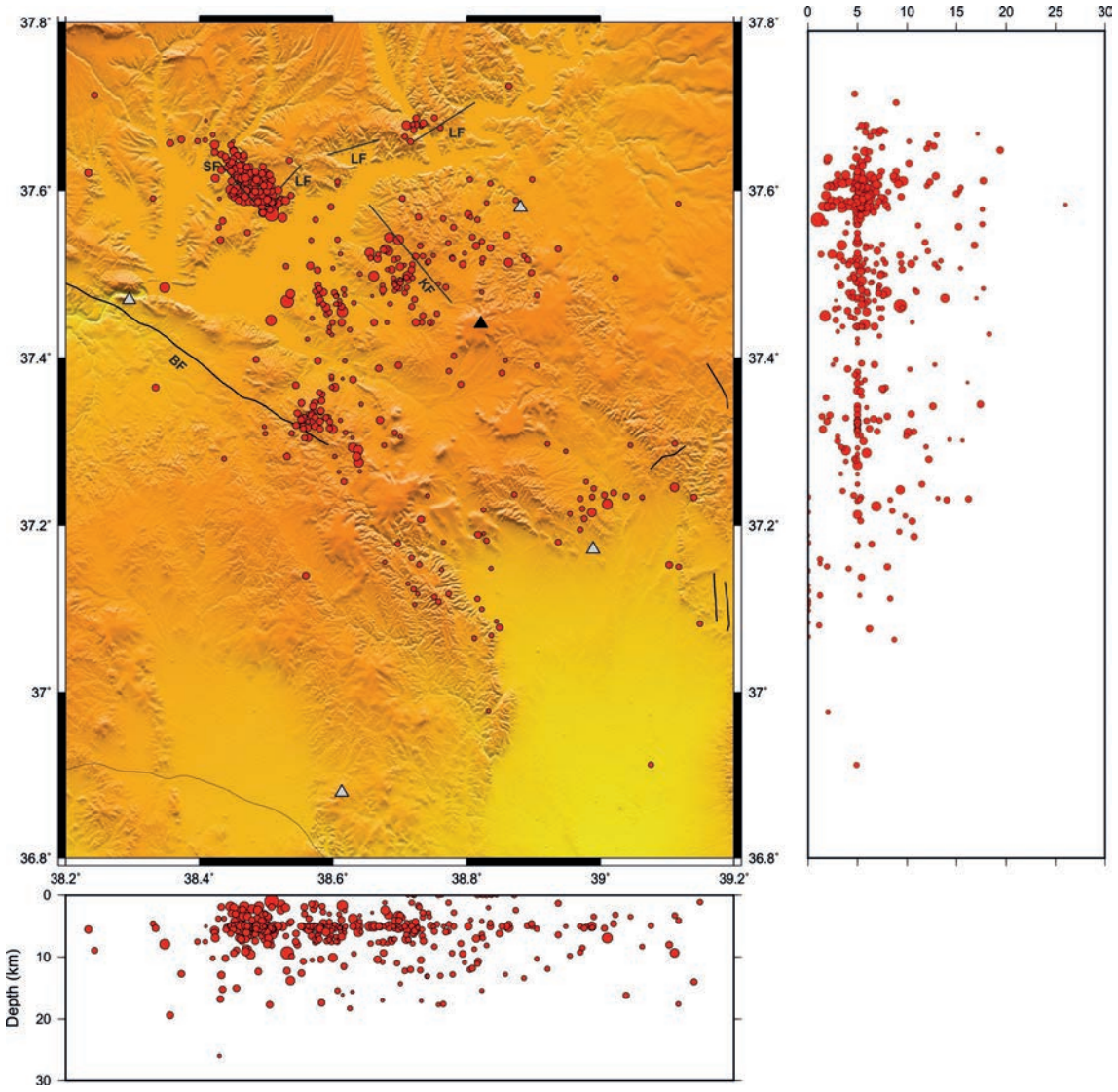

Fig. 7 - Earthquake locations obtained by combining KOERI and DEMP data. BF: Bozova Fault, SF: Samsat Fault, LF: Lice Fault, KF: Kalecik Fault.

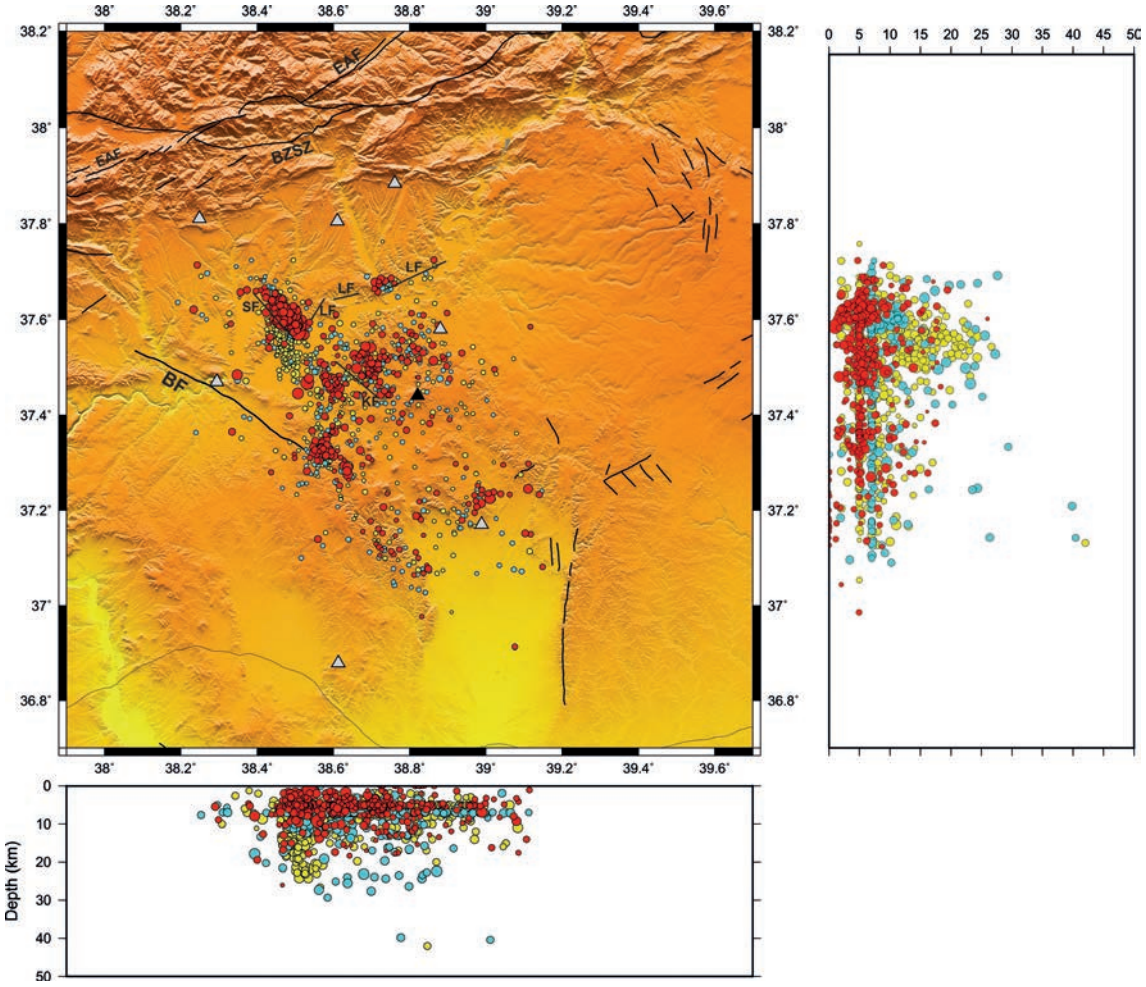

Fig. 8 - Comparison of the epicentres and hypocentres located by KOERI (yellow), DEMP (blue) and obtained from this study (red). White and black triangles indicate DEMP and KOERI stations, respectively. EAF: East Anatolian Fault, BZSZ: Bitlis Zagros Suture Zone, BF: Bozova Fault, SF: Samsat Fault, LF: Lice Fault, KF: Kalecik Fault.

earthquakes were located around Samsat Fault and the SW part of the Bozova and Kalecik faults. Also, a small cluster was observed at the northern part of the Lice Fault. The overall trend of the seismicity was NNW-SSE. Some of the lineations in the seismicity did not seem to be related to any of the known active faults in the region. Additionally, there was no seismic activity associated with the NW part of the Bozova Fault. Some of the scattering seismicity patterns located could be due to large azimuthal gaps of these earthquakes during location process or may be a result of small shocks that occurred randomly in space in the southern part of the study area. The computational errors (ERH, ERZ, RMS) of all the 434 events are given in Fig. 9.

Similarly, the epicentral distribution of the relocated events as well as the depth distribution of the analysed events were improved after the relocation process. It was determined that earthquakes in the study area mostly occur in continental areas (Fig. 7) rather than the Atatürk Dam and in Samsat peninsula at very shallow depths (mostly within the first 10 km of the crust). However, there are enough hypocentres where the depth retained its initial value (e.g. 4 or 5 km). This is

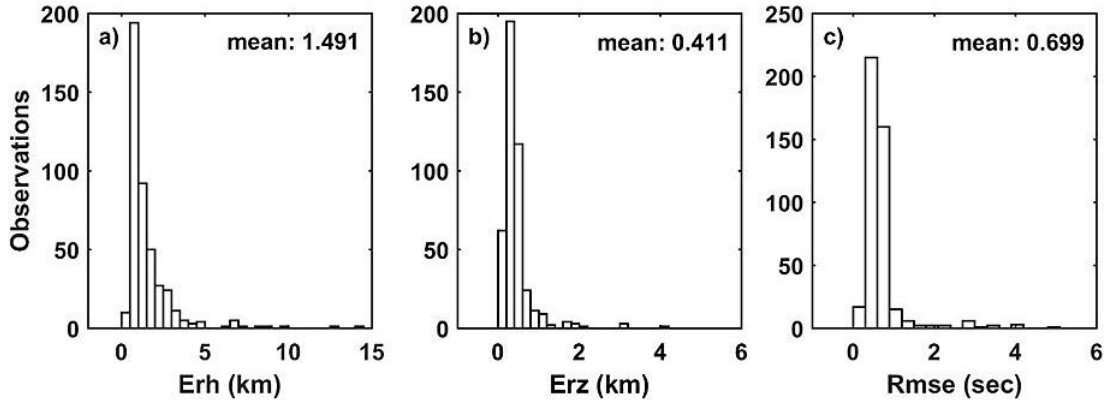

Fig. 9 - The computations error for all 434 events (ERH: horizontal error, ERZ: vertical error, RMS: root mean square error).

indicative of the low quality of these solutions, probably due to either the small number of P- and S-arrivals or the azimuthal distribution of the recording stations, or both.

Considering the magnitude of the earthquakes, the considerable damage during the 2017 and 2018 earthquake sequence in and around Samsat town could be explained by the shallow focal depths of the earthquakes (İmamoğlu *et al*., 2017; Özcan *et al*., 2017). The depth distribution of the analysed earthquakes in the study area indicated that both the maximum seismicity and depth of the seismicity increased from south to north and this behavior suggested crustal thickening due to plate tectonics (collision of the Arabian and Eurasian plates).

Fig. 10 summarises the results of the fault plane solutions for the analysed earthquakes obtained from first motion polarities and regional moment tensor analysis. The fault mechanism solutions

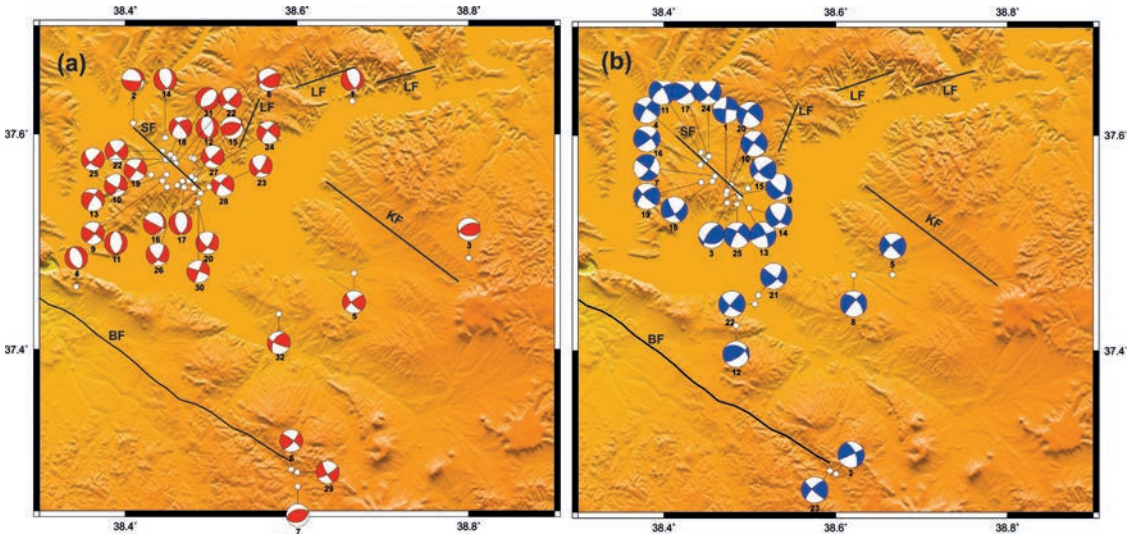

Fig. 10 - Focal mechanism obtained from: a) first motion polarity analysis and b) regional moment tensor analysis of the analysed events.

acquired as a result of both the first motion polarities and the regional moment tensor analysis were generally compatible, even though there were small differences in fault dipping. Strike-slip faulting was identified as the dominant mechanism after a careful analysis of the distribution of focal mechanisms of earthquakes in the study area. However, normal and reverse faulting components were observed in the strike-slip faulting mechanism. The focal mechanisms with reverse component were principally located in the eastern part of the studied region. Nonetheless, focal mechanisms of the analysed earthquakes that occurred in the northern part of the study area showed a more complicated tectonic structure which is an indication that the deformation pattern observed in this part of the study area is complex and heterogeneous. The earthquakes occurring in the northern part of the study area had strike-slip mechanism with normal component and normal faulting mechanism with right-lateral strike-slip component. The NE-SW trending nodal planes of the earthquakes in the western edge of the Samsat peninsula, where the Lice Fault and Samsat Fault intersect, may be related with the left-lateral strike-slip Lice Fault (earthquake number 3, 9, 13, 14, 15, 25 in Table 3 and Fig. 10b). All the focal mechanisms had a NW-SE or NE-SW nodal plane compatible with the regional geological trend.

Fig. 11 shows the present day stress tensor analysis results obtained by using focal mechanisms of earthquakes occurring in and around Samsat peninsula. The study area was represented by the strike-slip faulting regime, which was formed by the compressional regime. The resulting strike-slip faulting regime developed simultaneously or immediately after the compression regime. The stress regime index value ($R` = 1.64$) showed that the dominant regime in the Samsat peninsula and its surroundings is pure strike-slip.

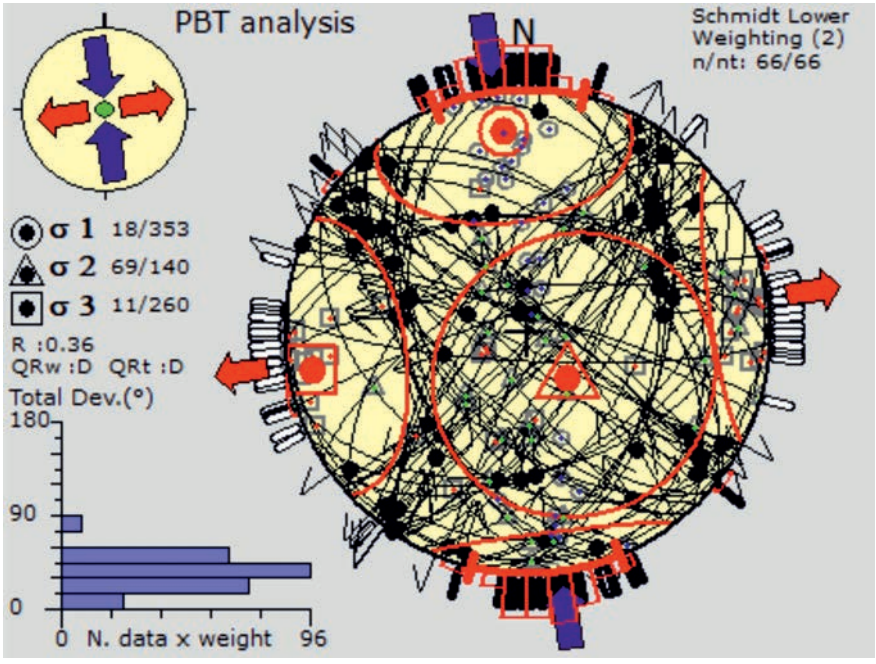

Fig. 11 - Present day deformation analysis for the Samsat peninsula.

5. Conclusion

The hypocentre parameters of the earthquakes in the Adıyaman-Samsat region and its vicinity were relocated by using both KOERI and DEMP data. The new locations of the earthquakes indicated that they are clustered in the Samsat peninsula, at the SW part of the Bozova Fault, whereas some epicentres of the earthquakes could be observed at the southern part of the study area. It was observed that earthquakes mostly occur in continental areas and Samsat peninsula at very shallow depths (mostly within the first 10 km of the crust). The depth distribution of the analysed earthquakes showed that both the maximum seismicity and depth of the seismicity increased from south to north and this behaviour indicates crustal thickening due to continental-continental collision in the study area. Focal mechanisms of the analysed earthquakes showed NW-SE trending strike-slip faulting with both normal and reverse component as the dominant mechanism in the study area. All the focal mechanisms had a NW-SE or NE-SW nodal plane compatible with the regional geological trend at the NE edge of the Samsat peninsula, where the Lice Fault and Samsat Fault intersect. The earthquakes that occurred at the NE edge of the Samsat peninsula could also be related to the left-lateral strike-slip Lice Fault (earthquake number 3, 9, 13, 14, 15, 25). However, the mainshocks of 2017 and 2018 and their aftershocks were consistent with the Samsat Fault rather than the Lice Fault. Some scatter of the seismicity pattern could be due to a laterally heterogeneous velocity structure. Therefore, 3D seismic tomography could be used to resolve lateral velocity structure in the study area.

Acknowledgements. The authors would like to thank Eleftheria Papadimitriou (editor), George Karakaisis and an anonymous reviewer for their helpful comments that improved the manuscript. The authors would also like to thank Mutala Mohammed (CSIR-IIR, Ghana) for proof reading the manuscript. The authors thank KOERI and DEMP for sharing earthquake data. This work was supported by the Scientific and Technological Research Council of Turkey (TÜBİTAK). Grant No: 117Y309.

REFERENCES

Bott M.H.P.; 1959: *The mechanics of oblique slip faulting*. Geol. Mag., **96**, 109-117.

Delvaux D.; 1993: *The TENSOR program for reconstruction: examples from the east African and the Baikal Rift systems*. Terra Abstr. Suppl. n. 1, Terra Nova, **5**, 216.

Delvaux D. and Sperner B.; 2003: *Stress tensor inversion from fault kinematic indicators and focal mechanism data: the TENSOR program*. In: Nieuwland D. (ed), New Insights into Structural Interpretation and Modelling, Geol. Soc. London, London, England, Spec. Publ., Vol. 212, pp. 75-100.

Dreger D.S.; 2003: *TDMT_INV: time domain seismic moment tensor inversion*. In: Lee W., Kanamori H., Jennings P. and Kisslinger C. (eds), International Handbook of Earthquake and Engineering Seismology, Part B, Academic Press, San Diego, CA, USA, Vol. 81B, p. 1627.

Dreger D.S. and Helmberger D.; 1991: *Source parameters of the Sierra Madre earthquake from regional and local body waves*. Geophys. Res. Lett., **18**, 2015-2018.

Dreger D.S. and Helmberger D.V.; 1993: *Determination of source parameters at regional distances with three-component sparse network data*. J. Geophys. Res.: Solid Earth, **98**, 8107-8125.

Dreger D.S. and Kaverina A.; 2000: *Seismic remote sensing for the earthquake source process and near-source strong shaking: a case study of the October 16, 1999 Hector Mine earthquake*. Geophys. Res. Lett., **27**, 1941-1944.

Dreger D.S., Ritsema J. and Pasyanos M.; 1995: *Broadband analysis of the 21 September, 1993 Klamath Falls earthquake sequence*. Geophys. Res. Lett., **22**, 997-1000.

Ertunç A.; 1999: *The geological problems of the large dams constructed on the Euphrates River (Turkey)*. Eng. Geol., **51**, 167-182.

Gee L.S., Neuhauser D.S., Dreger D.S., Pasyanos M.E., Uhrhammer R.A. and Romanowicz B.; 1996: *Real-time seismology at UC Berkeley: the rapid earthquake data integration project*. Bull. Seismol. Soc. Am., **86**, 936-945.

Gephart J.W. and Forsyth D.W.; 1984: *An improved method for determining the regional stress tensor using earthquake focal mechanism data: application to the San Fernando earthquake sequence*. J. Geophys. Res.: Solid Earth, **89**, 9305-9320.

Herrmann R.B. and Wang C.Y.; 1985: *A comparison of synthetic seismograms*. Bull. Seismol. Soc. Am., **75**, 41-56.

İmamoğlu Ş., Bedirhanoğlu İ., Öncü M.E. and Şimşek Z.; 2017: *02 Mart 2017 Adıyaman Samsat depremi ön değerlendirme raporu*. Dicle Üniversitesi, Mühendislik Fakültesi, Diyarbakır, Turkey.

Irmak T.S.; 2013: *Focal mechanisms of small-moderate earthquakes in Denizli Graben (SW Turkey)*. Earth, Planets and Space, **65**, 943.

Irmak T.S.; 2016: *Present-day stress field in the Bala-Ankara (Turkey) region from inversion of focal mechanisms*. East. Anatolian J. Sci., **2**, 37-48.

Jost M.U. and Herrmann R.B.; 1989: *A student's guide to and review of moment tensors*. Seismol. Res. Lett., **60**, 37-57.

Kalafat D., Gürbüz C. and Uçer B.; 1987: *Investigation of the crust and upper mantle in the west of Turkey*. Deprem Arastirma Bulteni, **14**, 43-64, (in Turkish).

Kartal R.F. and Kadirioğlu F.T.; 2019: *Impact of regional tectonic and water stress on the seismicity in Ataturk Dam Basin: southeast of Turkey*. J. Seismol., **23**, 699-714, doi: 10.1007/s10950-019-09830-5.

KOERI; 2019: *Kandilli Observatory and Earthquake Research Institute Data Centre*. Istanbul, Turkey, <www.koeri.boun.edu.tr/sismo/2/deprem-verileri/sayisal-veriler/> (last access: 12 April 2019).

Langston C.A.; 1981: *Source inversion of seismic waveforms: the Koyna, India, earthquakes of 13 September 1967*. Bull. Seismol. Soc. Am., **71**, 1-24.

Lee W.H.K. and Lahr J.C.; 1975: *Hypo71 (revised): a computer program for determining hypocenter, magnitude and first motion pattern of local earthquakes*. U.S. Department of the Interior, Geological Survey, National Center for Earthquake Research, Reston, VA, USA, Open file report 75-311, 113 pp.

Lienert B.R., Berg E. and Frazer L.N.; 1986: *HYPOCENTER: an earthquake location method using centered, scaled, and adaptively damped least squares*. Bull. Seismol. Soc. Am., **76**, 771-783.

Okay A.I., Zattin M. and Cavazza W.; 2010: *Apatite fission-track data for the Miocene Arabia-Eurasia collision*. Geol., **38**, 35-38.

Özcan Z., Mert N., Özocak A., Utkucu M. and Doğan E.; 2017: *2 Mart 2017 Samsat (Adıyaman) depremi ön değerlendirme raporu*. Sakarya Üniversitesi Rektörlüğü Afet Yönetim Uygulama ve Araştırma Merkezi.

Pasyanos M.E., Dreger D.S. and Romanowicz B.; 1996: *Toward real-time estimation of regional moment tensors*. Bull. Seismol. Soc. Am., **86**, 1255-1269.

Perinçek D. and Çemen I.; 1990: *The structural relationship between the East Anatolian and Dead Sea fault zones in southeastern Turkey*. Tectonophys., **172**, 331-340.

Perinçek D. Günay Y. and Kozlu H.; 1987: *New observations on strike-slip faults in east and southeast Anatolia*. In: Proc., 7th Biannual Petroleum Congress of Turkey, UCTEA Chamber of Petroleum Engineers, Turkish Association of Petroleum Geologists, Ankara, Turkey, pp. 89-103.

Reilinger R., McClusky S., Vernant P., Lawrence S., Ergintav S., Cakmak R., Ozener H., Kadirov F., Guliev I., Stepanyan R., Nadariya M., Hahubia G., Mahmoud S., Sakr K., ArRajehi A., Paradissis D., Al-Aydrus A., Prilepin M., Guseva T., Evren E., Dmitrotsa A., Filikov S.V., Gomez F., Al-Ghazzi R. and Karam G.; 2006: *GPS constraints on continental deformation in the Africa-Arabia-Eurasia continental collision zone and implications for the dynamics of plate interactions*. J. Geophys. Res.: Solid Earth, **111**, B05411, doi: 10.1029/2005JB004051.

Romanowicz B., Dreger D.S., Pasyanos M. and Uhrhammer R.; 1993: *Monitoring of strain release in central and northern California using broadband data*. Geophys Res. Lett., **20**, 1643-1646.

Şahbaz N. and Seyitoğlu G.; 2018: *The neotectonics of NE Gaziantep: the Bozova and Halfeti strike-slip Faults and their relationships with blind thrusts, Turkey*. Bull. Mineral Res. Explor., **156**, 17-40, doi: 10.19111/bulletinofmre.401216.

Saikia C.K.; 1994: *Modified frequency-wavenumber algorithm for regional seismograms using Filon's quadrature: modelling of Lg waves in eastern North America*. Geophys. J. Int., **118**, 142-158.

Scherbaum F.; 1994: *Basic concepts in digital signal processing for seismologists*. Springer-Verlag, Lecture Notes in Earth Sciences, Berlin/Heidelberg, Germany, Vol. 53, 158 pp.

Shomali H.Z. and Slunga R.; 2000: *Body wave moment tensor inversion of local earthquakes: an application to the south Iceland seismic zone*. Geophys. J. Int., **140**, 63-70.

Snoke J.A., Munsey J.W., Teague A.G. and Bollinger G.A.; 1984: *A program for focal mechanism determination by combined use of polarity and SV-P amplitude ratio data*. Earthquake Notes, **55**, 15.

Sperner B., Muller B., Heidbach O., Delvaux D., Reinecker J. and Fuchs K.; 2003: *Tectonic stress in the Earth's crust: advances in the world stress map project*. In: Nieuwland D.A. (ed), New insights in structural interpretation and modelling, Geol. Soc. London, London, England, Spec. Publ., Vol. 212, pp. 101-116.

Tatar O., Koçbulut F., Polat A. and Demirel M.; 2019: *02.03.2017 ve 24.04.2018 Samsat (Adıyaman) depremleri ve bölgesel sismotektonik içindeki önemi*. Türkiye Jeoloji Bülteni, **62**, 167-180.

Taymaz T., Eyidoğan H. and Jackson J.; 1991: *Source parameters of large earthquakes in the East Anatolian Fault zone (Turkey)*. Geophys. J. Int., **106**, 537-550.

Yilmaz Y., Yiğitbaş E. and Genç Ş.C.; 1993: *Ophiolitic and metamorphic assemblages of southeast Anatolia and their significance in the geological evolution of the orogenic belt*. Tectonics, **12**, 1280-1297.

Corresponding author: T. Serkan Irmak
Dept. of Geophysics, Seismology Section, Kocaeli University
Umuttepe Campus, 41100 Kocaeli, Turkey
Phone: +90 262 3033118; e-mail: irmakts@kocaeli.edu.tr